

The $H\alpha$ and Infrared Star Formation Rates for the Nearby Field Galaxy Survey

Lisa J. Kewley¹

Harvard-Smithsonian Center for Astrophysics

lkewley@cfa.harvard.edu

Margaret J. Geller

Smithsonian Astrophysical Observatory

Rolf A. Jansen

Dept. of Physics & Astronomy, Arizona State University

Mike Dopita

Research School of Astronomy and Astrophysics, Australian National University

ABSTRACT

We investigate the $H\alpha$ and infrared star formation rate (SFR) diagnostics for galaxies in the Nearby Field Galaxy Survey (NFGS). For the 93 galaxies in our sample, we derive $H\alpha$ fluxes (included here) from integrated spectra which typically cover 82% of each galaxy. There is a strong correlation between the ratio of infrared to optical star-formation rates $\text{SFR}(\text{IR})/\text{SFR}(\text{H}\alpha)$ and the extinction $E(B - V)$ measured with the Balmer decrement. Before reddening correction, the $\text{SFR}(\text{IR})$ and $\text{SFR}(\text{H}\alpha)$ are related to each other by a power-law: $\text{SFR}(\text{IR}) = (3.6 \pm 0.2) \text{SFR}(\text{H}\alpha)^{1.25 \pm 0.05}$. Correction of the $\text{SFR}(\text{H}\alpha)$ for extinction using the Balmer decrement and a classical reddening curve both reduces the scatter in the $\text{SFR}(\text{IR})$ - $\text{SFR}(\text{H}\alpha)$ correlation and results in a much closer agreement between the two SFR indicators; $\text{SFR}(\text{IR}) = (1.29 \pm 0.06) \text{SFR}(\text{H}\alpha_{\text{corr}})^{1.02 \pm 0.03}$.

This SFR relationship spans 4 orders of magnitude and holds for all Hubble types with IRAS detections in the NFGS. A constant ratio between the $\text{SFR}(\text{IR})$ and $\text{SFR}(\text{H}\alpha)$ for all Hubble types, including early types (S0-Sab), suggests that the IR emission in all of these objects results from a young stellar population.

Subject headings:

¹CfA Fellow

1. Introduction

Understanding the star formation history of the universe is the primary goal of much current research in astronomy (for example, Rowan-Robinson 2001; Cole et al. 2001; Baldry et al. 2002; Lanzetta et al. 2002; Rosa-González, Terlevich, & Terlevich 2002). To obtain this understanding, a reliable estimate of the star formation rate in individual galaxies is required. Many calibrations of star-formation rate depend on the luminosity measured at various wavelengths including: radio (eg., Condon 1992; Cram et al. 1998; Haarsma et al. 2000), IR (eg., Hunter et al. 1986; Lehnert & Heckman 1996; Meurer et al. 1997; Kennicutt 1998), optical (eg., Gallagher et al. 1989; Leitherer & Heckman 1995; Kennicutt 1998; Madau, Pozzetti, & Dickinson 1998; Rosa-González, Terlevich, & Terlevich 2002), or UV (eg., Buat, Deharveng & Donas 1989; Deharveng et al. 1994; Leitherer, Robert, & Heckman 1995; Meurer et al. 1995; Cowie et al. 1997; Madau, Pozzetti, & Dickinson 1998; Rosa-González, Terlevich, & Terlevich 2002). Unfortunately, the agreement among the SFR indicators at these different wavelengths is poor, and the underlying reasons for the differences are not well understood. To compute the SFR at any redshift and to relate SFRs at different redshifts, it is crucial to understand the physics underlying each SFR indicator and the source of the discrepancies among them.

Here, we investigate two SFR indicators, the SFR(IR) and SFR(H α), for a large, objectively selected sample of nearby galaxies. We aim to: (1) reduce the discrepancy between these two SFRs, and (2) obtain a better understanding of the relationship between the IR and H α emission for all Hubble types.

In star-forming galaxies, H α photons are produced by gas ionized by young hot stars. The SFR(H α) is then a direct measure of the current SFR in galaxies, provided that reddening is not significant. The SFR(H α) should agree with the SFR(IR) if the IR emission in star-forming galaxies arises from dust heated by the young hot stars. This scenario occurs in IR luminous starbursts (eg. Dopita et al. 2002), but the IR emission in normal star-forming galaxies appears more complex.

The IR emission (8–1000 μ m) in normal star-forming galaxies may arise from three processes: (1) the emission from dust heated by young OB stars (Devereux & Young 1990; Devereux & Hameed 1997); (2) the emission from the photospheres or circumstellar envelopes of evolved stars such as red-giants undergoing mass-loss (Knapp, Gunn, & Wynn-Williams 1992; Mazzei & de Zotti 1994); (3) the “cirrus” emission from dust distributed throughout the optically thin, neutral interstellar medium, heated by the general stellar radiation field. The general stellar radiation field is composed of a combination of unabsorbed radiation from young OB stars inside the active star-forming regions (eg., Zurita, Rozas, & Beckman 2000), and an underlying old stellar population consisting of A, F and G dwarfs, and K and

M giants (eg., Drapatz 1979; Helou 1986; Lonsdale & Helou 1987; Sauvage & Thuan 1994; Mazzei & de Zotti 1994). The relative contribution to the general stellar radiation field by the young and old stellar populations is unclear and may vary substantially from galaxy to galaxy depending on the details of the physical and dynamical environment and metallicity.

The calibration of infrared luminosity as an indicator of the global star formation rate in a galaxy relies upon two assumptions; (a) that young stars dominate the radiation field throughout the UV to the visible (ie., that processes (2) and (3) above are negligible), and (b) that the dust opacity is infinite throughout a galaxy. If these assumptions hold, then the IR luminosity approximates the bolometric luminosity of the galaxy, and the SFR(IR) is a reliable estimate of the true SFR of the galaxy.

For infrared-bright dusty star-forming galaxies, the young stellar population does produce the dominant dust heating radiation field, and the dust opacity is high (Lonsdale & Helou 1987; Poggianti, Bressan, & Franceschini 2001; Dopita et al. 2002; Rosa-González, Terlevich, & Terlevich 2002). Therefore, assumptions (a) and (b) above hold, and IR luminosity is a more direct indicator of the true SFR than the $H\alpha$ luminosity. Recently, Dopita et al. (2002) (hereafter D02) and Rosa-González, Terlevich, & Terlevich (2002) (hereafter R02) showed that using the Balmer decrement to correct the $H\alpha$ luminosity for reddening results in better agreement between the SFR(IR) and SFR($H\alpha$). The D02 sample contains merging infrared starburst galaxies; the R02 sample consists of nearby young star-forming galaxies, most are low metallicity late-type spirals or blue compact dwarfs. It is unclear from these results whether the approximate agreement between SFR(IR) and SFR($H\alpha$) after reddening correction also applies to a wider range of “normal” galaxies.

The young (OB) star-forming population dominates the IR emission in late-type spirals. The nature of the IR emission in early-type spirals, on the other hand, remains controversial. Dust heating by the general stellar radiation field may make a significant contribution to the IR emission in early-types (eg., Lonsdale & Helou 1987; Sauvage & Thuan 1994; Mazzei & de Zotti 1994) bringing the use of SFR(IR) into question for these galaxies. Early-type galaxies may have small dust opacities further complicating the use of SFR(IR).

Kennicutt & Kent (1983) demonstrated that the $H\alpha$ equivalent width increases systematically from early-type to late-type galaxies. This increase suggests that early-type galaxies are deficient in young stars. Sauvage & Thuan (1994) provide additional evidence for this deficiency. They found that the $B - V$ and $U - B$ colors decrease and the ratio of H I mass to blue luminosity increases systematically from S0 to Im type in the CfA1 galaxy sample (Davis & Peebles 1983; Huchra et al. 1983). Furthermore, IR SED modeling of early-types appears to require a cooler component to the IR emission (Buat & Deharveng 1988; Rowan-Robinson & Crawford 1989), often attributed to the general stellar radiation field.

An intriguing theoretical argument by Inoue (2002) suggests that the SFR(IR) can be applied to a wide range of galaxy types, including those with an older stellar population and small dust opacity. Inoue proposes a scenario in which the two effects of small dust opacity and a large cirrus contribution offset each other, making the SFR(IR) a good measure of the true SFR within a factor of 2 for a wide range of galaxy types.

Although the general stellar radiation field may be important in many early-type spirals, $H\alpha$ images provide convincing evidence that at least some early-type galaxies contain significant recent star formation (Hameed & Devereux 1999). In addition, Tomita, Tomita & Saito (1996) and Devereux & Hameed (1997) showed that the far infrared-to-blue luminosity ratio is independent of Hubble type for a large sample of nearby spirals. Their work supports the idea that early-type galaxies contain substantial recent star formation.

A number of studies compare various SFR indicators for normal disk galaxies (eg., Kennicutt 1983; Hopkins et al. 2001; Charlot et al. 2002; Buat et al. 2002). Most of these authors cannot properly correct the $H\alpha$ luminosity for reddening or stellar absorption because they lack integrated optical spectra with sufficient spatial coverage, signal-to-noise, and wavelength coverage. For example, Charlot et al. (2002) use had to assume an ‘average’ attenuation $A_v = 1$ for the galaxies in the Stromlo-APM survey where the slit-covering fraction is 40-50 percent.

In this paper, we analyze integrated spectra from the Nearby Field Galaxy Survey (NFGS) (Jansen et al. 2000a), described in Section 2. We ensure that the integrated $H\alpha$ luminosity is properly corrected for reddening and underlying stellar absorption. We compare uncorrected SFR($H\alpha$) with SFR(IR) in Section 3. Section 4 compares the corrected SFR($H\alpha$) with the SFR(IR). The agreement between the two SFR indicators in the latter section is remarkable and is independent of Hubble type. We discuss the implications of this agreement in Section 5.

2. Sample selection and cross-correlation with IRAS

The NFGS is ideal for investigating relative IR and $H\alpha$ star formation rates. The sample was selected objectively from the CfA1 galaxy survey (Davis & Peebles 1983; Huchra et al. 1983) with $m_{B(0)} < 14.5$. The CfA1 catalog is nearly complete within its selection limits and contains galaxies with a large range of absolute magnitude ($-22 \lesssim M_z \lesssim -13$). Jansen et al. (2000a) chose a subsample of 198 nearby galaxies spanning the full range of Hubble type and absolute magnitude present in the CfA1 catalog. To avoid a strict diameter limit, which might introduce a bias against the inclusion of low surface brightness galaxies in the

sample, they chose a radial velocity limit, $V_{\text{LG}}(\text{km s}^{-1}) > 10^{-0.19-0.2M_z}$ (with respect to the Local Group standard of rest). To avoid a sampling bias favoring a cluster population, they excluded galaxies in the direction of the Virgo Cluster. The absolute magnitude distribution in the NFGS sample approximates the local galaxy luminosity function, while the distribution over Hubble type follows the changing mix of morphological types as a function of luminosity in the local galaxy population. Low surface brightness galaxies are overrepresented in the NFGS relative to the CfA1 sample.

Both integrated and nuclear spectrophotometry are available for almost all galaxies in the NFGS sample, including reliably measured integrated $\text{H}\alpha$ and $\text{H}\beta$ fluxes relative to the flux at 5500\AA (Jansen et al. 2000b; Jansen, Franx, & Fabricant 2001). The spectra have high enough S/N ratios to measure the $\text{H}\beta$ fluxes even when $E(B-V)$ is large.

The integrated spectra typically cover $82 \pm 7\%$ of the galaxy. We calibrate the integrated fluxes, $F_{\text{rel}}(\lambda)$, to absolute fluxes, $F(\lambda)$, by careful comparison with B -band photometry. We converted total B -magnitudes (extrapolated to infinite radius) to flux densities, $F(4350\text{\AA}, \text{phot})$, at the effective wavelength of the B -filter (4350\AA). The uncertainties in the constant relating the magnitude to the flux of Vega, and in the effective wavelength of the B -filter for a given galaxy SED are $\sim 2\text{-}3\%$ combined. Because the position, size and orientation of the spectroscopic apertures are known, the B -filter galaxy images allow us to compute the fractions, f , of the total B -filter light that enters the spectroscopic apertures with $1.5\text{-}3\%$ accuracy. The mean value of $f = 0.82 \pm 0.07$. The B -filter flux density to which we must scale the spectra is then

$$F(B, \text{spec}) = f \times F(4350\text{\AA}, \text{phot}).$$

Scaling the relatively flux calibrated spectrum, $F_{\text{rel}}(\lambda)$, by the ratio of this flux density and that derived from the spectrum itself, we obtain the absolute flux calibrated spectrum:

$$F(\lambda) = F_{\text{rel}}(\lambda) \cdot \frac{F(B, \text{spec})}{\langle F_{\text{rel}}(\lambda) \otimes T_B(\lambda) \rangle} \quad [\text{erg s}^{-1} \text{cm}^{-2} \text{\AA}^{-1}] ,$$

where $\langle F_{\text{rel}}(\lambda) \otimes T_B(\lambda) \rangle$ denotes the mean relative flux density, derived by convolving the relative spectrum with the normalized B -filter response curve (Bessell 1979). The maximum error in the relative flux calibration is $\sim 6.5\%$. The range in uncertainty in the total B -filter magnitudes is $\sim 1\text{-}10\%$, with a mean of 3.0% and rms of 2.7% . The errors in the absolute flux calibration of the spectrum are smallest at 4350\AA and increase toward both shorter and longer wavelengths. The expected error in the derived absolute $\text{H}\alpha$ ($\text{H}\beta$) emission line fluxes is on average $\sim 12\%$ ($\sim 17\%$) and at most $\sim 34\%$ ($\sim 50\%$) for galaxies with $\text{EW}(\text{H}\beta) \lesssim -0.5\text{\AA}$. The error in the $\text{H}\beta$ flux is larger than that in $\text{H}\alpha$, because the $\text{H}\beta$ emission line is fainter and its measurement is complicated by the superposition of stellar absorption.

As described in Jansen, Franx, & Fabricant (2001), the line fluxes are corrected for Galactic extinction, using Burnstein & Heiles (1984; as listed in de Vaucouleurs et al. 1991). The $H\beta$ emission is partially corrected for stellar absorption by ensuring that the limits of the flux measurement window are well inside the absorption trough, closely bracketing the emission line. We evaluated the residual absorption using spectra of galaxies without detectable emission. On average, we applied an additional correction of 1.0\AA in equivalent width (EW) to $H\beta$ and 1.5\AA EW to $H\alpha$.

We cross-correlated the NFGS with the IRAS Faint Source Catalogue (FSC) and Point Source Catalogue (PSC). The IRAS beam size at $60\text{ }\mu\text{m}$ is 1.5 arcminutes, and the IRAS positional uncertainty is 30 arcseconds. Because the NFGS positional uncertainty is only a few arcseconds and because all but a few of the NFGS galaxies are smaller than 3 arcmin in extent, we used a detection radius of 30 arcseconds. Any IRAS source associated with an NFGS object should be detected within this radius. We found 110 (56%) NFGS galaxies with IRAS sources within 30 arcseconds; 99 of these galaxies have $H\alpha$ fluxes accurate to within 30%, and 97 have $H\beta$ fluxes accurate to within 30%.

To rule out the presence of AGN in the NFGS sample, we used the theoretical optical classification scheme developed by Kewley et al. (2001). The optical diagnostic diagrams indicate that the global spectra of 93/97 NFGS galaxies are dominated by star formation. These 93 galaxies constitute the sample we analyse here. We list the galaxies in Table 1. The spectra of the remaining 4 galaxies are dominated by AGN: A00510+1225, A12195+7535, A15016+1037 and NGC 5940 host Seyfert I nuclei.

3. Infrared versus $H\alpha$ SFRs

The development of SFR diagnostics has been an intense topic of research for over three decades (see Kennicutt 1998, for a review) (hereafter K98). We use the K98 SFR relations for IR and $H\alpha$ because these relations are used in many current SFR studies. We defer a more detailed analysis of other SFR diagnostics to a future paper.

The IR SFR relation (K98) depends on the infrared luminosity (L_{IR}) from the 12, 25, 60, and $100\text{ }\mu\text{m}$ IRAS fluxes computed following Sanders & Mirabel (1996):

$$L_{\text{IR}} = 4\pi D_L^2 F_{\text{IR}} \quad (1)$$

where D_L is the cosmological "luminosity distance". We assume $H_0 = 75\text{ km s}^{-1}\text{ Mpc}^{-1}$ and $q_0 = 0.5$. F_{IR} is the infrared flux of the source, defined as

$$F_{\text{IR}} = 1.8 \times 10^{-14} (13.56F_{12} + 5.26F_{25} + 2.54F_{60} + F_{100}) \text{ Wm}^{-2} \quad (2)$$

where F_{12} , F_{25} , F_{60} , F_{100} are the IRAS fluxes of the galaxies at 12, 25, 60 and 100 microns respectively.

The IR SFR relation (K98) is:

$$\text{SFR}(\text{M}_{\odot}\text{yr}^{-1}) = 4.5 \times 10^{-44} L_{\text{IR}} (\text{ergs s}^{-1}). \quad (3)$$

(note that the 8-1000 μm luminosity L_{IR} is defined as L_{FIR} in K98). This standard SFR relation assumes that young stars dominate the radiation field throughout the UV-visible regimes, and that the optical depth is large. The infrared luminosity is then a good representation of the bolometric luminosity of the galaxy. Although this situation may hold for IR-luminous starburst galaxies, it does not necessarily apply to normal galaxies where the emission may be dominated by emission from a cooler, “infrared cirrus” component (eg., Lonsdale & Helou 1987).

The $\text{H}\alpha$ SFR relation (K98) comes from evolutionary synthesis models, assuming solar metallicity and no dust. The total integrated stellar luminosity shortward of the Lyman limit is re-emitted in the nebular emission lines. The $\text{H}\alpha$ SFR relation is:

$$\text{SFR}(\text{M}_{\odot}\text{yr}^{-1}) = 7.9 \times 10^{-42} L(\text{H}\alpha) (\text{ergs s}^{-1}) \quad (4)$$

For most star-forming galaxies, dust absorption leads to the underestimation of the SFR derived from the $\text{H}\alpha$ luminosity (eg., Lonsdale & Helou 1987).

Figure 1 shows the SFRs derived using the K98 IR and $\text{H}\alpha$ SFR relations for the NFGS galaxies. There is obviously a strong correlation between the two SFRs. Upper limits for those objects with measurable $\text{H}\alpha$ fluxes but without IRAS detections are consistent with this correlation. We fit a straight line to the logarithm of the SFRs for the objects with IRAS detections using the numerical recipes *fityx* routine in IDL. This routine uses linear least-squares minimization and includes error estimates for both variables. We assumed errors of $\sim 60\%$ for the non-reddening corrected $\text{SFR}(\text{H}\alpha)$ and $\sim 30\%$ for $\text{SFR}(\text{IR})$. The large $\sim 60\%$ error allows for the systematic error introduced by failure to correct for reddening. The resulting fit (dotted line in Figure 1) has the form:

$$\log[\text{SFR}(\text{IR})] = (1.25 \pm 0.06) \log[\text{SFR}(\text{H}\alpha)] + 0.56 \pm 0.05 \quad (5)$$

or:

$$\text{SFR}(\text{IR}) = (3.6 \pm 0.2) \text{SFR}(\text{H}\alpha)^{1.25 \pm 0.05}. \quad (6)$$

The rms distance perpendicular to this line (in the log) gives a measure of the degree of scatter. The rms dispersion in Figure 1 is 0.17 in the log. The Spearman Rank correlation test for $\text{SFR}(\text{IR})$ and $\text{SFR}(\text{H}\alpha)$ gives a correlation coefficient of 0.94. The two-sided probability

of finding a value of 0.93 by chance is formally 0.0 ($\lesssim 10^{-30}$), confirming the very strong correlation between the two SFR indicators.

We plot a histogram of the ratio of the two SFRs $\log(\text{SFR}(\text{IR})/\text{SFR}(\text{H}\alpha))$, in Figure 2. Markers at the top of Figure 2 show the means of the early and late type SFR ratio distributions, 0.64 ± 0.06 and 0.48 ± 0.03 , respectively. We note that the mean for the early types is larger than the mean for the late types.

4. SFRs and Reddening

Figures 1 and 2, and equation 6 demonstrate that the $\text{SFR}(\text{IR})$ estimate exceeds $\text{SFR}(\text{H}\alpha)$ by more than a factor of ~ 3 , as observed by (Charlot et al. 2002). The ratio between $\text{SFR}(\text{IR})$ and $\text{SFR}(\text{H}\alpha)$ increases with SFR. If the $\text{SFR}(\text{IR})$ and $\text{SFR}(\text{H}\alpha)$ are both valid measures of the true SFRs, then a physical process not yet taken into account must bias one relative to the other. This process must also cause the bias to increase at higher SFRs. One obvious candidate is reddening. We test this conjecture by measuring the difference in the extinction at two wavebands, $E(B - V)$.

We calculated $E(B - V)$ in the emission-line gas for the 93 IRAS-detected galaxies in the NFGS sample for which flux measurements for both $\text{H}\alpha$ and $\text{H}\beta$ are available. We assume an intrinsic $\text{H}\alpha/\text{H}\beta$ ratio of 2.85 (case B recombination at $T = 10^4\text{K}$ and electron density $n_e \sim 10^2 - 10^4\text{cm}^{-3}$; (Osterbrock 1989) and used the Whitford reddening curve as parameterized by Miller & Mathews (1972).

Figure 3 shows the relationship between the ratio of the two SFR indicators $\text{SFR}(\text{IR})/\text{SFR}(\text{H}\alpha)$ and $E(B - V)$. The Spearman Rank correlation coefficient is 0.76. The two-sided probability of obtaining a value of 0.76 by chance is $\sim 1.6 \times 10^{-19}$, supporting the very strong correlation between $\text{SFR}(\text{IR})/\text{SFR}(\text{H}\alpha)$ and $E(B - V)$.

The *fityx* least squares line fitting routine gives

$$\log \left[\frac{\text{SFR}(\text{IR})}{\text{SFR}(\text{H}\alpha)} \right] = (0.79 \pm 0.06) \log[E(B - V)] + 0.57 \pm 0.08 \quad (7)$$

If we use $E(B - V)$ to correct $\text{SFR}(\text{H}\alpha)$ for extinction, the difference between $\text{SFR}(\text{IR})$ and $\text{SFR}(\text{H}\alpha)$ could be reduced, supporting similar results by Dopita et al. (2002) and Rosa-González, Terlevich, & Terlevich (2002) for young starforming galaxies. Infact, after making the correction, we do arrive at a much better agreement between the corrected $\text{H}\alpha$ star formation rate ($\text{SFR}(\text{H}\alpha_{\text{corr}})$) and the IR star formation rate (Figure 4). This relation is

striking because many nearby field galaxies are cool IRAS sources. Only 6 out of the 93 galaxies in Figure 4 have a $60\mu\text{m}$ to $100\mu\text{m}$ flux ratio greater than 0.6, typical for objects dominated by hot stars (Bothun, Lonsdale, & Rice 1989).

We fit a straight line to the NFGS data in Figure 4 using the same method as for Figure 1. The errors are $\sim 30\%$ for both $\text{SFR}(\text{H}\alpha)$ and $\text{SFR}(\text{IR})$. The resulting fit is

$$\log[\text{SFR}(\text{IR})] = (1.02 \pm 0.03) \log[\text{SFR}(\text{H}\alpha_{\text{corr}})] + 0.11 \pm 0.02 \quad (8)$$

or,

$$\text{SFR}(\text{IR}) = (1.29 \pm 0.06) \text{SFR}(\text{H}\alpha_{\text{corr}})^{1.02 \pm 0.03}. \quad (9)$$

The Spearman rank correlation coefficient for $(\text{SFR}(\text{H}\alpha_{\text{corr}}))$ and $\text{SFR}(\text{IR})$ is 0.97, with the 2-sided probability of obtaining this value of $\lesssim 10^{-30}$. The rms scatter of the data around this line decreases to 0.13 in the log. Clearly correcting $\text{H}\alpha$ for reddening results in a closer correspondence between $\text{SFR}(\text{IR})$ and $\text{SFR}(\text{H}\alpha)$, and reduces the scatter observed in Figure 1. The constant fractional offset of 0.29 could be caused by a calibration error in either of the two K98 SFR calibrations, or in the calibration of the $\text{H}\alpha$ or IR fluxes.

If the general stellar radiation field contributes significantly to the IR emission in early-types, we would expect the late-types to display a larger scatter than early types. We find the contrary: the rms scatter for the early-types (S0-Sab) is 0.09, compared to 0.14 for the late-types (Sb-Im).

We plot a histogram of the ratio of the two SFRs $\log(\text{SFR}(\text{IR})/\text{SFR}(\text{H}\alpha))$, in Figure 5. After correction for reddening, the means of the two SFR ratios for early and late types are approximately equal: 0.14 ± 0.03 and 0.10 ± 0.02 respectively. Greater reddening for the early types appears to explain the offset in Figure 2. The overall mean in the ratios is 0.11 ± 0.02 .

By selecting early-types with infrared detections, we bias our early-type sample towards galaxies with more recent star-formation than is normal in these galaxies. The number of early-types with IRAS detections is 20/59 (34%), compared with the number of late-types with detections 80/112 (71%). This detection rate supports the many previous studies which showed that early-types in general have less recent star formation than late types (eg., Kennicutt & Kent 1983; Sauvage & Thuan 1994). The strong agreement and very small scatter between $\text{SFR}(\text{IR})$ and $\text{SFR}(\text{H}\alpha)$ for the infrared early-types implies that they are dominated in both $\text{H}\alpha$ and the IR by recent star formation.

We obtain SFR estimates by multiplying the luminosity at the relevant wavelength by a constant. Thus, the SFR correlation (Figure 4) is really the result of a strong correlation between the logarithm of the infrared and $H\alpha$ luminosities. The line of best fit to the luminosity correlation is;

$$\log[L(\text{IR})] = (1.02 \pm 0.03)\log[L(H\alpha_{\text{corr}})] + (2.2 \pm 0.2) \quad (10)$$

or,

$$L(\text{IR})/L(H\alpha_{\text{corr}}) \sim 155 \pm 71. \quad (11)$$

For the K98 star formation rate indicators to produce equivalent IR and $H\alpha$ star formation rates, the ratio $L(\text{IR})/L(H\alpha_{\text{corr}})$ multiplied by the ratio of the constants in the K98 relations should be ~ 1 . Multiplying the ratio $L(\text{IR})/L(H\alpha_{\text{corr}})$ by the ratio of the K98 coefficients gives $(155 \pm 71) \times 0.0058 \sim 0.9 \pm 0.4$. Clearly, the ratio of the K98 coefficients is an excellent estimate of the relationship between $L(\text{IR})/L(H\alpha_{\text{corr}})$ and $\text{SFR}(\text{IR})/\text{SFR}(H\alpha_{\text{corr}})$.

It is interesting that such a strong IR- $H\alpha$ correlation occurs. In the simplest picture, the correlation indicates that a single physical process is responsible for both the IR and $H\alpha$ emission. In reality, the IR and $H\alpha$ radiation may be produced in quite different environments. The $H\alpha$ radiation comes from gas ionized by the UV radiation from young, hot OB stars. This process occurs within many H II regions throughout a galaxy. The IR radiation source is more complex. The IR luminosity is calculated from the flux within the four IRAS bands at 12, 25, 60 and 100 μm . Each band comes from dust grains at different temperatures, and may be associated with different types of regions within a galaxy.

The near to mid-infrared spectrum of most galaxies is composed of a featureless continuum and a family of aromatic bands, called the unidentified infrared bands (UIBs) (eg., Puget & Leger 1989). The continuum emission is attributed to very small grains, most likely heated by the radiation from young, hot stars inside H II regions (Cesarsky et al. 1996; Roussel et al. 2001). The UIB carriers could be carbonaceous molecules such as PAHs (Léger & Puget 1984), or aggregates of several hundred atoms (Boulanger et al. 1998; Draine 2001). The Infrared Space Observatory (ISO) resolved individual regions in our galaxy and revealed that the UIBs are closely associated with the photodissociation shells and surfaces of molecular clouds in the vicinity of H II regions or hot stars (Cesarsky et al. 1996; Roussel et al. 2001). These results strongly suggest that the 12 and 25 μm fluxes are dominated by the emission from young hot stars.

The far-IR spectra of galaxies result from large dust grains of diameter 0.01-0.3. The spectrum from these grains is characteristic of thermal emission at 15-20K (see Draine 2001,

for a review), and accounts for nearly all the emission at $\lambda > 60\mu\text{m}$. Some authors believe that an older stellar population can make a significant contribution to the far-IR emission (eg., Lonsdale & Helou 1987; Sauvage & Thuan 1994; Mazzei & de Zotti 1994) for early-type galaxies. However, our $\text{H}\alpha$ -LIR correlation implies that the dominant UV and optical heating source for this emission is the young stellar population. This hypothesis is in agreement with various other physical correlations linking the FIR emission to young stellar populations, such as the radio-FIR correlation (eg., Gavazzi, Cocito, & Vettolani 1986), and the $12\mu\text{m}$ -FIR luminosity correlation (Shapley, Fabbiano, & Eskridge 2001). Both of these correlations hold for all galaxy types.

These correlations suggest that the gas and dust must be closely coupled in all IR-bright galaxies. Malhotra et al. (2001) found a strong correlation between $L_{[\text{OI}]} / L_{[\text{CII}]}$ and $F(60\mu\text{m}) / F(100\mu\text{m})$, indicating that both gas and dust temperatures increase together. The most plausible explanation for this effect is that the majority of the dust and gas heating in galaxies occurs very close to the actively star-forming regions.

Modeling by Popescu & Tuffs (2002) for normal star-forming galaxies strengthens this explanation. The Popescu et al. models predict that radiation from H II regions is the dominant energy source for the dust emitting at $60\mu\text{m}$. Even at $100\mu\text{m}$, H II regions contribute $\sim 1/3$ of the radiation source. The other $2/3$ is produced by the diffuse UV and optical radiation, which could also contain some contribution from the young stellar population.

Even if the IR emission is dominated by the young stellar population, one would expect the ratio of gas and dust masses to vary from one H II region to another, and from one galaxy to another. Similarly, the dust geometry and composition must vary. If these variations occur, they do not appear to have an effect on the relationship between the global IR and $\text{H}\alpha$ luminosities.

5. Conclusions

We analyze a sample of 93 infrared detected galaxies from the Nearby Field Galaxy Survey. The NFGS is an objectively selected sample of galaxies in the CfA1 catalog. The sample contains a representative mix of all galaxy types and morphologies represented in the CfA1 survey. In addition, the NFGS is unique in the quality and coverage of the integrated spectra. We have taken extensive care to ensure that the integrated $\text{H}\alpha$ flux for each galaxy is as reliable as possible. We have corrected these fluxes carefully for extinction and underlying stellar absorption.

To compare the IR and $\text{H}\alpha$ star formation rates, we make the following standard as-

sumptions: (1) the Whitford reddening law is appropriate for all galaxies in our sample, and (2) the star formation rates are proportional to the relevant luminosities. After correction for extinction, the SFR(IR) is consistently $\sim 30\%$ larger than the SFR(H α).

With the assumed reddening, the data provide a direct measurement of the ratio of the IR and H α SFR constants which transform the luminosities to star formation rates, $\log[L(\text{IR})] = (1.02 \pm 0.03)\log[L(\text{H}\alpha_{\text{corr}})] + (2.2 \pm 0.2)$. The measured ratio is consistent with the ratio of the Kennicutt (1998) constants to within 30%.

Correction for reddening brings the mean of SFR(IR)/SFR(H α) for early and late types into agreement. One average, early types in this sample are more heavily reddened than late types. It is intriguing that the ratio between the SFR(IR) and SFR(H α) is the same for early and late types. The IR emission from early-type spirals may contain a significant contribution from the general stellar radiation field. This contribution should increase the observed IR luminosity. Inoue (2002) suggested that this effect is offset by a lower dust opacity. This compensation would require a remarkable conspiracy to hold for all galaxy types. The physical properties of dust and the nature of the general stellar radiation field probably vary from galaxy to galaxy. The variation in the general stellar radiation field should result in a larger dispersion around the SFR relation for early types than late-types. We do not observe this variation. Rather, the infrared NFGS early-type galaxies have a smaller dispersion than the late-types.

Previous studies have shown that early-type galaxies contain a lower fraction of young-to-old stellar populations than late-types (eg., Kennicutt & Kent 1983; Sauvage & Thuan 1994; Davis & Peebles 1983; Huchra et al. 1983). This result does not determine what combination of young-to-old populations produces the IR emission in each galaxy. The agreement of SFR(IR) with SFR(H α) for both early types and late-types implies that the IR emission results from the same young stellar population which produces the H α emission. This hypothesis is supported by other physical correlations linking the FIR emission to the young stellar population, including the radio-FIR correlation (Gavazzi, Cocito, & Vettolani 1986) and the $12\mu\text{m}$ -FIR luminosity correlation (Shapley, Fabbiano, & Eskridge 2001). These correlations suggest that the dust is heated in close proximity to the young star-forming regions. In addition, the FIR-H α correlation implies that the relationship between the global dust and gas properties is universal for all IRAS galaxies in the NFGS.

Further observations and modeling are required to prove that the young stellar population is responsible for FIR emission in all galaxy types, rather than a compensation effect as suggested by Inoue (2002). Near-infrared observations would enable separation of the young and old stellar populations. The Space Infrared Telescope Facility (SIRTF) will help determine whether the global dust and gas properties are truly universal for all IRAS galaxies in

the NFGS.

We enjoyed discussions about many aspects of this paper with Rob Kennicutt and Dan Fabricant. L. J. Kewley is supported by a Harvard-Smithsonian CfA Fellowship. M. J. Geller is supported by the Smithsonian Institution.

REFERENCES

- Baldry, I. K., et al. 2002, *ApJ*, 569, 582
- Binette, L., Magris, C. G., Stasinska, G., & Bruzual, A. G. 1994 *A&A*, 292, 13
- Bessell, M. S. 1979, *PASP*, 91, 589
- Bothun, G. D., Lonsdale, C. J., & Rice, W. 1989, *ApJ*, 341, 129
- Boulanger, F., Boissel, P., Cesarsky, D., & Ryter, C. 1998, *A&A*, 339, 194
- Buat, V., Boselli, A., Gavazzi, G. & Bonfanti, C. 2002, *A&A*, 383, 801
- Buat, V. & Deharveng, J. M. 1988, *A&A*, 195, 60
- Buat, V. & Deharveng, J. M., Donas, J. 1989, *A&A*, 223, 42
- Burstein, D., & Heiles, C. 1984, *ApJS*, 54, 33
- Cesarsky, D., Lequeux, J., Abergel, A., Perault, M., Palazzi, E., Madden, S., & Tran, D. 1996, *A&A*, 315, 309
- Charlot, S., Kauffman, G., Longhetti, M., Tresse, L., White, S. D. M., Maddox, S. J., & Fall, S. M. 2002, *MNRAS*, 330, 876
- Condon, J. J. 1992, *AR&A*, 30, 575
- Cole, S. et al. 2001, *MNRAS*, 326, 255
- Cowie, L. L., Hu, E. M., Songaila, A., & Egami, E. 1997, *ApJ*, 481, L9
- Cram, L., Hopkins, A., Mobasher, B., & Rowan-Robinson, M. 1998, *ApJ*, 507, 155
- Davis, M. & Peebles, P. J. M. 1983, *ApJ*, 267, 465

- Draine, B. T. 2001, “Interstellar Grains”, *Encyclopedia of Astronomy and Astrophysics* (IOP Publishing and McMillan), 1266-1273
- Drapatz, S. 1979, *A&A*, 75, 26
- Deharveng, J. M., Sasseen, T. P., Buat, V., Bowyer, S., & Lampton, M., & Wu, X. 1994, *A&A*, 289, 715
- de Vaucouleurs, G., de Vaucouleurs, A., Corwin, H. G., Jr., Buta, R. J., Paturel, G., & Fouqu, P. 1991, *Third Reference Catalogue of Bright Galaxies* (New York: Springer)
- Devereux, N. A. & Hameed, S. 1997, *AJ*, 113, 599
- Devereux, N. A. & Young, J. S. 1990, *ApJ*, 350, 25
- Dopita, M. A., Periera, L., Kewley, L. J., & Capacciolo, M. 2002, *ApJ*, in press
- Gallagher, J. S., Hunter, D. A., Bushouse, H. 1989, *AJ*, 97, 700
- Gavazzi, G., Cocito, A., & Vettolani, G. 1986, *ApJ*, 305, L15
- Haarsma, D. B., Partridge, R. B., Windhorst, R. A., & Richards, E. A. 2000, *ApJ*, 544, 641
- Hameed, S. & Devereux, N. 1999, *AJ*, 118, 730
- Helou, G. 1986, *ApJ*, 311, 33
- Hopkins, A. M., Connolly, J., Haarsma, D. B., & Cram, L. E. 2001, *AJ*, 122, 288
- Huchra, J., Davis, M., Latham, D., & Tonry, J. 1983, *ApJS*, 52, 89
- Hunter, D. A., Gillett, F. C., Gallagher, J. S., Rice, W. L., & Low, F. J. 1986, *ApJ*, 303, 171
- Inoue, A. K. 2002, *ApJ*, 570, 97
- Jansen, R. A., Franx, M., Fabricant, D., & Caldwell, N. 2000a, *ApJS*, 126, 271
- Jansen, R. A., Fabricant, D., Franx, M., & Caldwell, N. 2000b, *ApJS*, 126, 331
- Jansen, R. A., Franx, M., & Fabricant, D. 2001, *ApJ*, 551, 825
- Kennicutt, R. C., Jr 1983, *ApJ*, 272, 54
- Kennicutt, R. C. Jr., & Kent, S. M. 1983, *AJ*, 88, 1094
- Kennicutt, R. C. Jr. 1998, *ARA&A*, 36, 189

- Kewley, L. J., Heisler, C. A., Dopita, M. A., & Lumsden, S. 2001, *ApJS*, 132, 37
- Kewley, L. J., Dopita, M. A., Sutherland, R. S., Heisler, C. A., & Trevena, J. 2001, *ApJ*, 556, 121
- Knapp, G. R., Gunn, J. E., & Wynn-Williams, C. G. 1992, *ApJ*, 399, 76
- Lanzetta, K. M., Yahata, N., Pascarelle, S., Chen, H.-W., Fernández-Soto, A. 2002, *ApJ*, 570, 492
- Léger, A. & Puget, J. L. 1984, *A&A*, 137, L5
- Lehnert, M. D., & Heckman, T. M. 1996, *ApJ*, 472, 546
- Leitherer, C. & Heckman, T. 1995, *ApJS*, 96, 9
- Leitherer, C., Robert, C., & Heckman, T. 1995, *ApJS*, 99, 173
- Lonsdale, C. J. & Helou, G. 1987, *ApJ*, 314, 513
- Madau, P., Pozzetti, L., & Dickinson, M. 1998, *ApJ*, 498, 106
- Malhotra, S., Kaufman, M. J., Hollenbach, D., Helou, G., Rubin, R. H., Brauher, J., Dale, D., Lu, N. Y., Lord, S., Stacey, G., Contursi, A., Hunter, D. A., & Dinerstein, H. 2001, *ApJ*, 561, 766
- Mazzei, P. & de Zotti, G. 1994, *ApJ*, 426, 97
- Meurer, G. R., Heckman, T. M., Leitherer, C., Kinney, A., Robert, C., & Garnett, D. R. 1995, *AJ*, 110, 2665
- Meurer, G. R., Gerhard, R., Heckman, T. M., Lehnert, M. D., Leitherer, C., & Lowenthal, J. 1997, *AJ*, 114, 54
- Miller, J. S., & Mathews, W. G. 1972, *ApJ*, 172, 593
- Osterbrock, D. E. 1989, *Astrophysics of Gaseous Nebulae and Active Galactic Nuclei* (Mill Valley; University Science Books)
- Shapley, A., Fabbiano, G., & Eskridge, P. B. 2001, *ApJS*, 137, 139
- Poggianti, B. M., Bressan, A., & Franceschini, A. 2001, *ApJ*, 550, 195
- Popescu, C. & Tuffs, R. J. 2002, *astro-ph/0203123*

- Puget, J. L. & Leger 1989, ARA&A, 27, 161
- Rosa-González, D., Terlevich, E., & Terlevich, R. 2002, MNRAS, 332, 283
- Roussel, H., Sauvage, M., & Vigroux, L., Bosma, A. 2001, A&A, 372, 427
- Rowan-Robinson, M. 2001, ApJ, 549, 745
- Rowan-Robinson, M. & Crawford, J. 1989, MNRAS, 238, 523
- Sanders, D. B., & Mirabel, I. F. 1996, ARA&A, 34, 749
- Sauvage, M. & Thuan, T. X. 1994, ApJ, 429, 153
- Tomita, A., Tomita, Y., & Saito, M. 1996, PASJ, 48, 285
- Zurita, A., Rozas, M., & Beckman, J. E. 2000, A&A, 363, 9

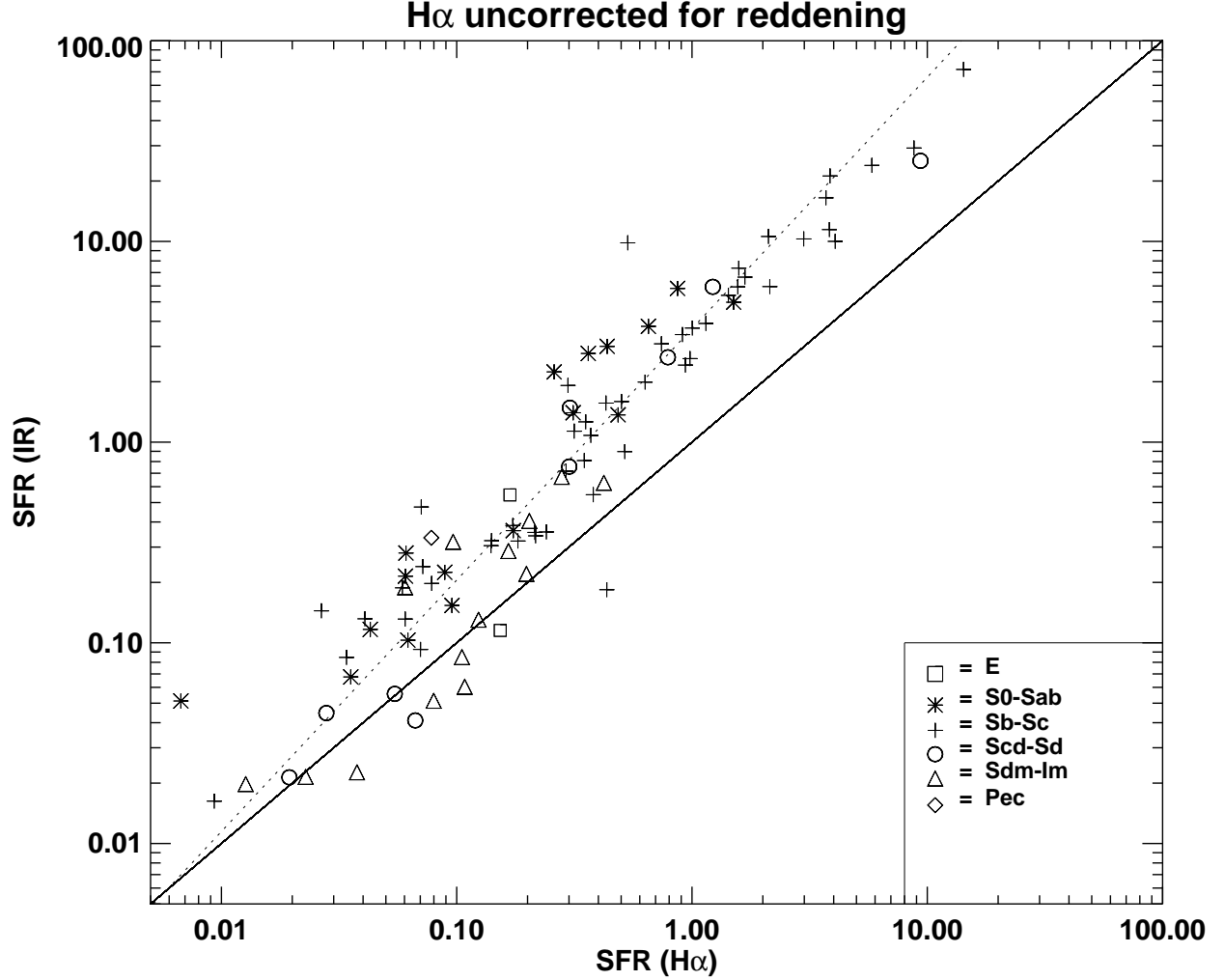


Fig. 1.— A comparison of the SFRs derived using the infrared and H α relations in Kennicutt (1998). The strong correlation spans 4 orders of magnitude. The solid line is $y=x$, and shows where the data would lie if both SFR indicators agreed. The H α SFR has not been corrected for extinction. The dashed line is the best-fit to all of the data. The legend indicates the Hubble type.

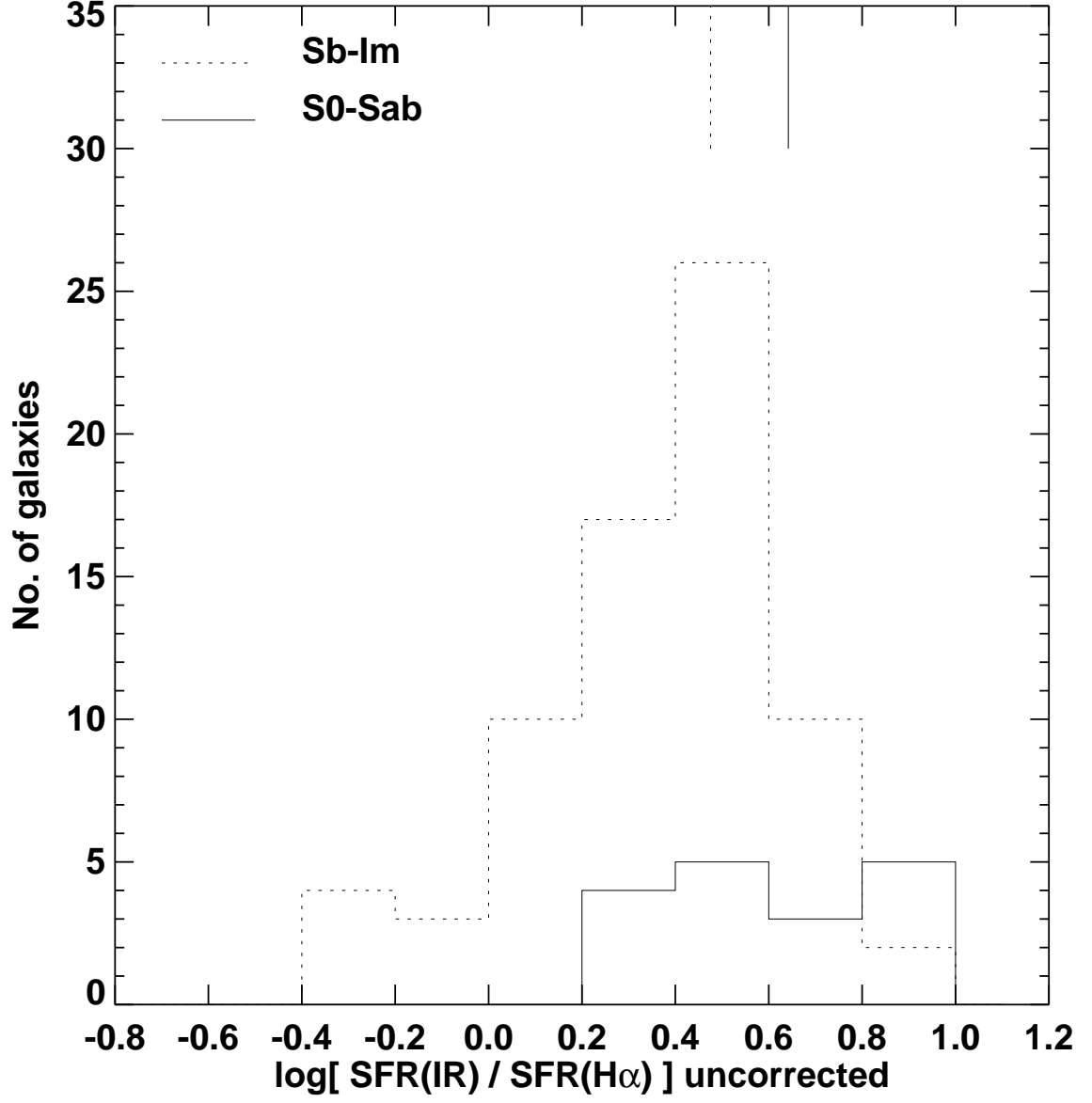


Fig. 2.— The ratio of the infrared to H α star formation rates. The H α flux has not been corrected for reddening. The two vertical lines at the top of the Figure indicate the mean of the early and late-type distributions.

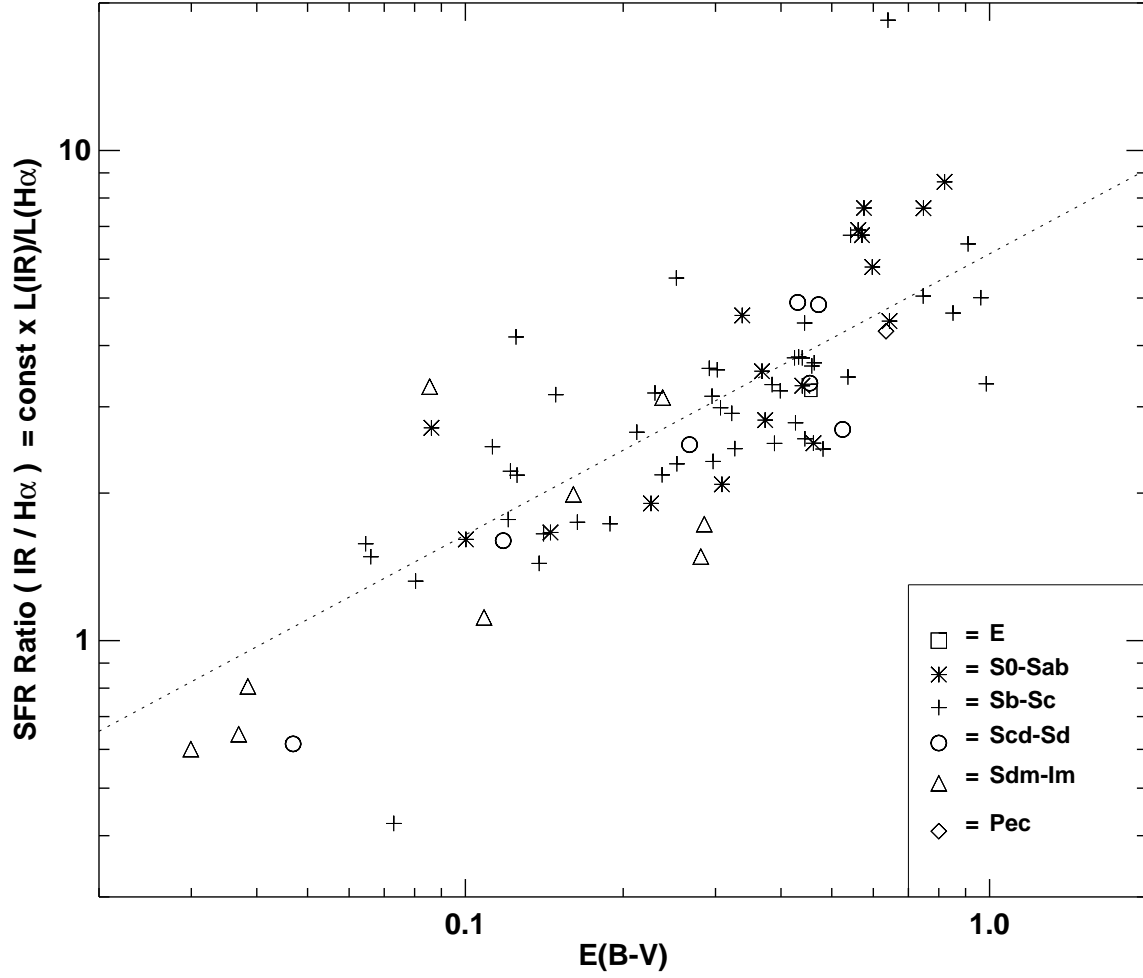


Fig. 3.— The relationship between the reddening $E(B - V)$ derived from the Balmer decrement $F(\text{H}\alpha)/F(\text{H}\beta)$ and the ratio of the IR to $\text{H}\alpha$ star formation rates.

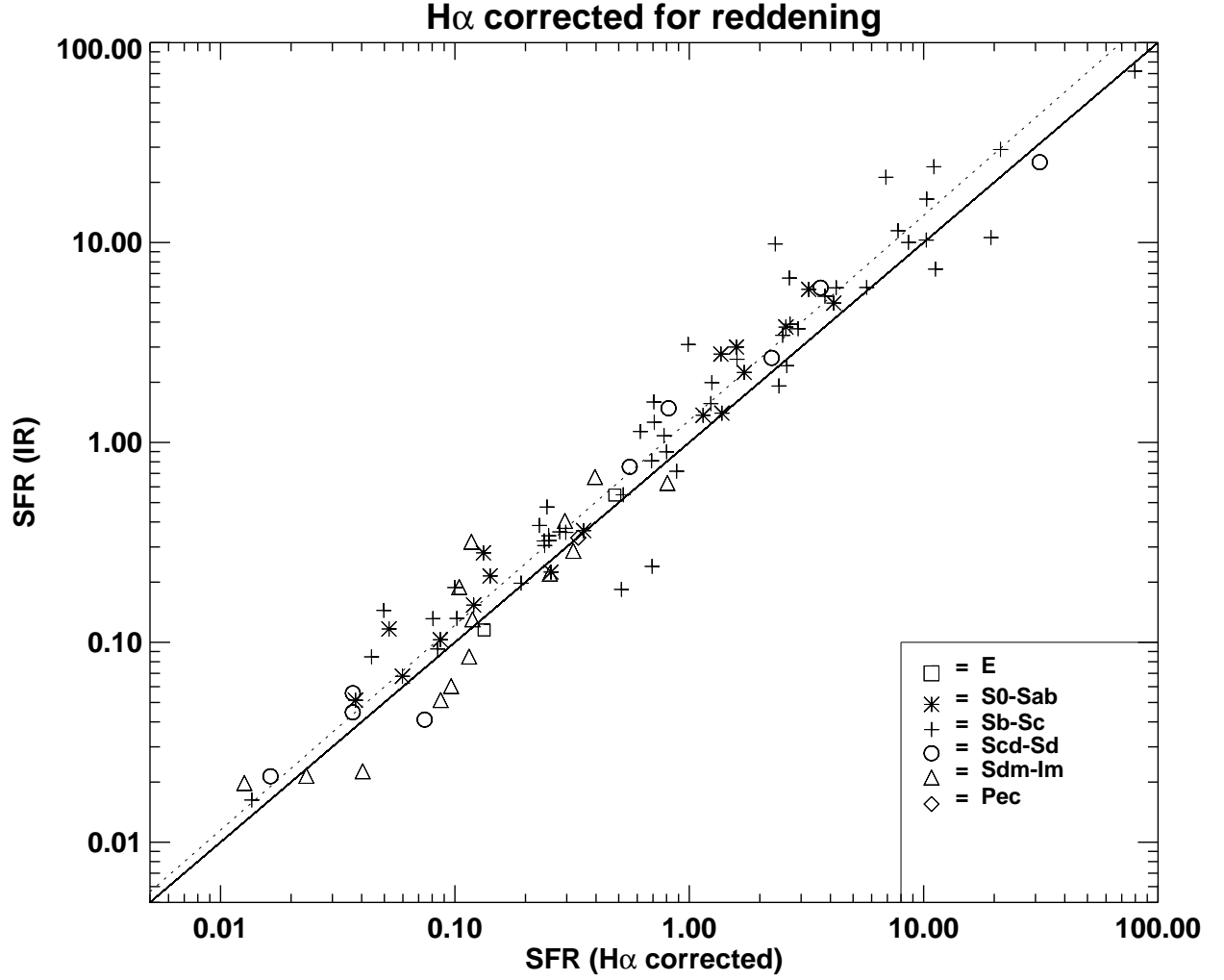


Fig. 4.— As in Figure 1, with the H α flux corrected for reddening using the Whitford reddening curve as parameterized by Miller & Mathews (1972). The SFR(IR) and SFR(H α) are nearly equal. The legend indicates the Hubble types. The galaxies with the largest SFRs are late-type spirals.

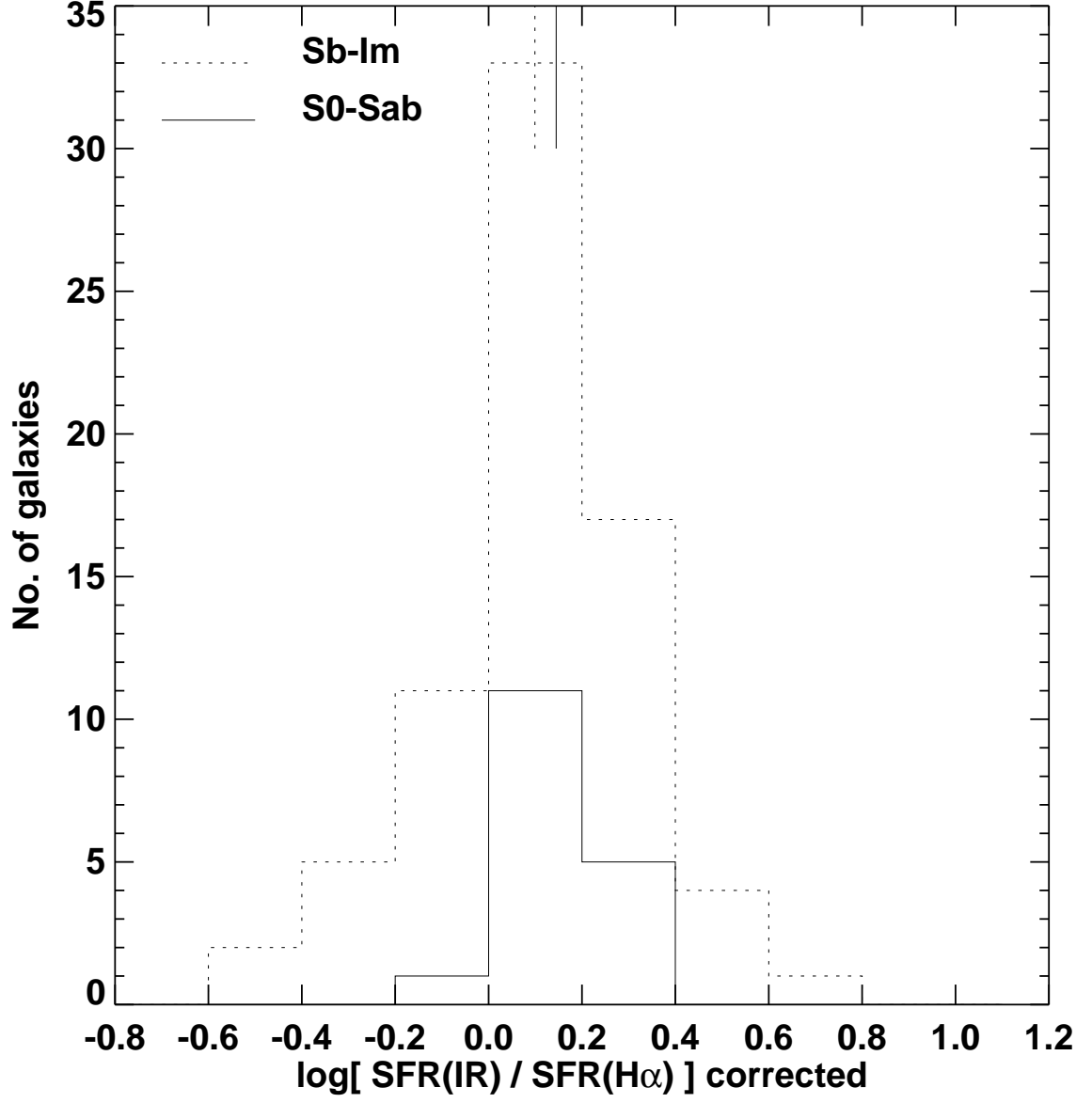


Fig. 5.— The ratio of the infrared to H α star formation rates. The H α flux has been corrected for reddening. The two vertical lines at the top of the Figure indicate the mean of the early and late-type distributions.

Table 1. The NFGS Sample with IRAS detections

ID	Name	cz (km/s)	Type	$E(B - V)$	$\frac{F(H\alpha)}{1 \times 10^{-13}}$	$\frac{F_{\text{corr}}(H\alpha)}{1 \times 10^{-13}}$	SFR(H α)	SFR _{corr} (H α)	SFR(IR)
4	A00389-0159	5302	Sa	0.44	3.13	8.60	1.50	4.13	4.98
5	A00442+3224	4859	Sb	0.37	2.84	6.66	1.15	2.69	3.90
8	A00570+1504	5517	Sab	0.56	0.84	3.05	0.44	1.59	3.00
16	A01344+2838	7756	Sbc	0.43	2.07	5.53	2.14	5.72	5.96
17	A01346+0438	3158	Sbc	0.30	2.05	4.06	0.35	0.69	0.81
19	NGC 695	9705	Sc	0.75	8.79	49.1	14.3	79.7	72.0
21	A02008+2350	2669	Sdm	0.28	3.48	6.65	0.42	0.81	0.63
23	IC 197	6332	Sbc	0.42	2.08	5.52	1.43	3.79	5.39
24	IC 1776	3405	Sc	0.19	2.62	4.05	0.52	0.80	0.90
25	A02056+1444	4405	Sb	0.44	2.75	7.55	0.91	2.50	3.44
27	NGC 927	8258	Sc	0.54	2.54	8.75	2.98	10.3	10.3
28	A02257-0134	1762	Sdm	0.24	1.14	1.98	0.06	0.10	0.19
37	A08567+5242	9036	Sb	0.96	1.50	13.78	2.11	19.4	10.6
39	NGC 2780	1951	Sab	0.34	0.94	2.04	0.06	0.13	0.28
43	NGC 2844	1486	Sa	0.37	1.61	3.77	0.06	0.14	0.21
44	NGC 3011	1517	S0/a	0.09	1.10	1.34	0.04	0.05	0.12
45	NGC 3009	4666	Sc	0.30	0.95	1.91	0.35	0.71	1.26
46	IC 2520	1226	.. / Pec	0.46	6.59	18.84	0.17	0.48	0.55
47	A09557+4758	1172	Sm	0.04	4.51	4.93	0.11	0.11	0.08
48	NGC 3075	3566	Sc	0.15	2.31	3.26	0.50	0.71	1.59
49	A09579+0439	4185	Sb	0.46	1.44	4.13	0.43	1.24	1.56
50	NGC 3104	604	Im	0.03	6.09	6.52	0.04	0.04	0.02
53	A10114+0716	1228	Sc	0.08	2.74	3.29	0.07	0.08	0.09
55	A10171+3853	2008	Sm	0.09	1.41	1.71	0.10	0.12	0.32
56	NGC 3213	1412	Sbc	0.40	1.20	3.01	0.04	0.10	0.13
57	NGC 3264	929	Sdm	0.00	7.37	6.57	0.10	0.10	0.06
58	NGC 3279	1422	Sc	0.54	2.06	7.18	0.07	0.25	0.47
59	A10321+4649	3338	Sc	0.29	1.66	3.25	0.32	0.62	1.13
60	A10337+1358	2997	Scd	0.43	1.98	5.33	0.30	0.82	1.48
61	IC 2591	6755	Sbc	0.20	2.14	3.42	1.68	2.67	6.64
63	A10368+4811	1534	Sc	0.13	1.51	2.01	0.06	0.08	0.13
65	A10389+3859	10693	Sbc	0.64	0.27	1.18	0.53	2.33	9.84
70	NGC 3454	1153	Sc	0.23	2.60	4.42	0.06	0.10	0.19
73	NGC 3510	704	Sd	0.05	7.92	8.83	0.07	0.07	0.04
76	A11017+3828W	2204	Sc	0.06	2.62	3.04	0.22	0.25	0.34
77	IC 673	3851	Sa	0.37	1.92	4.53	0.49	1.15	1.37
82	NGC 3633	2553	Sa	0.82	2.34	15.46	0.26	1.72	2.24
88	A11336+5829	1225	Sc	0.11	1.33	1.73	0.03	0.04	0.08
89	NGC 3795A	1154	Scd	0.00	2.41	1.62	0.05	0.04	0.06
90	A11372+2012	10964	Sc	0.28	2.80	5.33	5.82	11.1	23.9
91	NGC 3795	1091	Sc	0.27	1.31	2.46	0.03	0.05	0.14
94	NGC 3846	1396	Sm	0.00	3.74	3.59	0.12	0.12	0.13
96	A11476+4220	1033	S0	0.23	1.96	3.29	0.04	0.06	0.07
98	IC 746	5027	Sb	0.30	1.46	2.89	0.63	1.25	1.99
100	NGC 3978	9978	Sbc	0.38	5.11	12.39	8.77	21.3	29.2
105	A12001+6439	1447	S0	0.31	4.88	9.94	0.17	0.35	0.36
107	NGC 4120	2251	Sc	0.14	2.49	3.45	0.21	0.30	0.35
109	NGC 4141	1980	Sc	0.07	6.51	7.70	0.43	0.51	0.18

Table 1—Continued

ID	Name	cz (km/s)	Type	$E(B - V)$	$\frac{F(H\alpha)}{1 \times 10^{-13}}$	$\frac{F_{\text{corr}}(H\alpha)}{1 \times 10^{-13}}$	SFR(H α)	SFR _{corr} (H α)	SFR(IR)
110	NGC 4159	1761	Sdm	0.29	3.14	6.07	0.17	0.32	0.29
112	NGC 4238	2771	Sc	0.14	2.91	4.00	0.38	0.52	0.55
114	A12167+4938	3639	Sc	0.32	1.64	3.45	0.37	0.78	1.08
121	A12295+4007	685	Sd	0.00	2.44	2.05	0.02	0.02	0.02
122	A12300+4259	540	Sdm	0.008	4.61	4.70	0.02	0.02	0.02
124	NGC 4509	907	Sm	0.04	5.71	6.22	0.08	0.09	0.05
125	A12331+7230	6959	Sb	0.43	1.88	5.10	1.57	4.24	5.94
127	NGC 4758	1244	Sbc	0.39	2.98	7.28	0.08	0.19	0.20
133	A13065+5420	2460	Sb	0.07	2.33	2.72	0.24	0.28	0.36
134	IC 4213	815	Scd	0.12	2.48	3.25	0.03	0.04	0.04
135	A13194+4232	3396	Scd	0.27	1.53	2.83	0.30	0.56	0.76
137	NGC 5173	2467	E	0.63	0.75	3.24	0.08	0.34	0.33
140	NGC 5230	6855	Sc	0.33	5.04	10.7	4.06	8.61	10.0
141	A13361+3323	2364	Sm	0.16	2.14	3.10	0.20	0.29	0.40
142	NGC 5267	5941	Sb	0.91	0.49	3.99	0.30	2.41	1.92
144	NGC 5338	777	S0	0.75	0.66	3.67	0.007	0.04	0.05
145	NGC 5356	1397	Sb	0.99	2.16	20.9	0.07	0.69	0.24
148	NGC 5425	2062	Sc	0.24	1.93	3.34	0.14	0.24	0.30
151	NGC 5491	5845	Sc	0.46	1.72	4.98	1.00	2.91	3.70
153	NGC 5541	7698	Sc	0.44	3.64	10.1	3.71	10.3	16.5
155	NGC 5608	662	Sm	0.00	1.71	1.70	0.01	0.01	0.02
156	A14305+1149	2234	Sc	0.12	2.14	2.83	0.18	0.24	0.32
158	NGC 5762	1788	Sa	0.10	1.76	2.21	0.10	0.12	0.15
159	A14489+3547	1215	Pec	0.00	6.10	5.31	0.15	0.13	0.12
161	IC 1066	1613	Sab	0.46	2.01	5.81	0.09	0.26	0.22
162	A14594+4454	626	Sc	0.16	1.40	2.04	0.009	0.02	0.02
164	IC 1100	6561	Scd	0.47	1.66	4.92	1.23	3.63	5.94
165	NGC 5874	3128	Sbc	0.48	1.75	5.30	0.29	0.88	0.72
166	NGC 5875A	2470	Sc	0.12	1.67	2.21	0.17	0.23	0.38
168	IC 1124	5242	Sab	0.60	1.39	5.50	0.65	2.58	3.78
170	A15314+6744	6461	Sc	0.21	1.37	2.23	0.98	1.60	2.61
171	NGC 5993	9578	Sb	0.25	2.44	4.37	3.86	6.90	21.2
172	IC 1141	4458	S0/a	0.58	1.07	4.02	0.36	1.36	2.77
174	NGC 6007	10548	Sbc	0.31	2.00	4.05	3.84	7.78	11.5
175	A15523+1645	2191	Sc	0.25	1.72	3.08	0.14	0.25	0.32
179	NGC 6131	5054	Sc	0.12	1.70	2.26	0.74	0.99	3.09
181	NGC 7077	1142	S0/a	0.15	2.80	3.91	0.06	0.09	0.10
184	NGC 7328	2827	Sab	0.64	2.29	10.1	0.31	1.38	1.40
186	A22426+0610	1925	Sdm	0.15	4.43	6.28	0.30	0.40	0.67
187	A22551+1931N	5682	S0	0.57	1.57	5.85	0.87	3.23	5.83
189	NGC 7460	3296	Sb	0.44	5.06	14.07	0.94	2.61	2.42
192	A23176+1541	4380	Sd	0.45	2.41	6.86	0.79	2.25	2.65
193	NGC 7620	9565	Scd	0.52	5.93	19.8	9.35	31.3	25.2
195	IC 1504	6306	Sb	0.85	2.32	16.5	1.58	11.2	7.36
198	A23542+1633	1788	Im	0.11	3.64	4.67	0.20	0.25	0.22